Title

Modeling Electrolyte Composition Effects on Anion-Exchange-Membrane Water Electrolyzer Performance

Journal

ECS Transactions, 92(8)

ISSN

1938-5862

Authors

Stanislaw, Lauren N

Gerhardt, Michael R

Weber, Adam Z

Publication Date

2019-07-03

DOI

10.1149/09208.0767ecst

Peer reviewed

Modeling Electrolyte Composition Effects on Anion-Exchange Membrane Water Electrolyzer Performance

Lauren N. Stanislaw, Michael R. Gerhardt, and Adam Z. Weber

[a] Energy Conversion Group, Lawrence Berkeley National Laboratory, Berkeley, California 94720, USA

Anion-exchange membrane (AEM) water electrolysis could allow inexpensive and greener hydrogen production than other alternatives, such as steam methane reforming. To increase performance, hydroxide salts are often added to the water feed, with the tradeoff of corrosivity and complexity. Recently, carbonate salts that are less corrosive have shown promise, but their specific functionality remains unknown. In this paper, we use a mathematical model to compare an AEM electrolyzer with added potassium carbonate to an AEM electrolyzer with added potassium hydroxide. We show that the conductivity of the carbonate-form membrane has little impact on the performance of the device, but that carbonate ions replace hydroxide in the ionomer, which creates a Nernstian voltage difference across the membrane. The replacement of hydroxide anions with carbonate also reduces utilization of the catalyst in the anode, resulting in an additional voltage loss.

Introduction

Currently, 95% of hydrogen produced in the United States is produced via steam methane reforming, in which steam and methane react to produce hydrogen and carbon dioxide (1). Steam methane reforming is a developed technology, but because it relies on fossil fuels and releases carbon dioxide into the atmosphere, the environmental advantages of using hydrogen fuel are partially negated.

Water electrolysis using renewable electricity can produce hydrogen without greenhouse gas emissions. Two main water-electrolysis technologies have enjoyed some commercial success: alkaline electrolysis and proton-exchange membrane (PEM) electrolysis. In alkaline electrolysis, electrodes are placed in a hydroxide solution and current is passed to generate hydrogen. Alkaline electrolysis utilizes inexpensive nickel-based catalysts, but due to the permeability of the porous separators typically used, production of pressurized hydrogen is difficult (2). PEM electrolysis uses a PEM such as Nafion® to separate hydrogen from oxygen, allowing for differential pressure operation. Because the PEM is strongly acidic, however, PEM electrolysis relies on the use of expensive precious-metal catalysts such as platinum (3).

AEM electrolysis combines the catalyst flexibility of alkaline environments with the ability to produce pressurized hydrogen (4). In an AEM electrolyzer (Figure 1), water is electrochemically converted into hydrogen and oxygen:

$$2H_2O \rightarrow O_2 + 2H_2 \quad [1]$$

Typically, in an AEM electrolyzer, water is fed to the anode, where it transports across the AEM to the cathode. At the cathode catalyst layer (CL), water is reduced into hydroxide and hydrogen (Equation 2). The hydrogen then leaves the device through the cathode gas diffusion layer (GDL), where it can be captured. Meanwhile, the hydroxide transports through the membrane to reach the anode CL, where it is oxidized (Equation 3). The products are oxygen, which diffuses through the anode GDL, and a small amount of water, which can transport back through the membrane toward the cathode.

$$4H_2O + 4e^- \rightarrow 2H_2 + 4OH^-,\ E^0 = -0.8277\ \text{V vs SHE}, \quad [2]$$
$$4OH^- \rightarrow O_2 + 2H_2O + 4e^-,\ E^0 = +0.401\ \text{V vs SHE}. \quad [3]$$

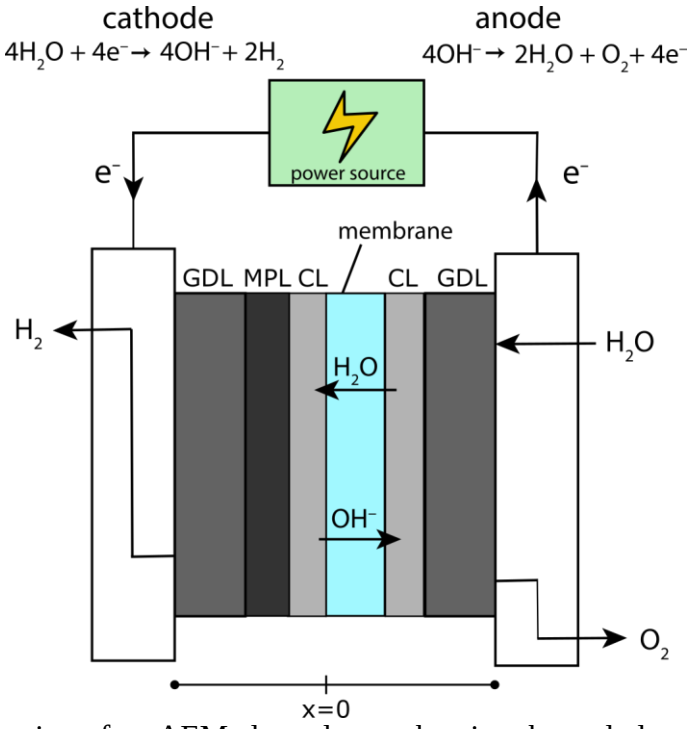

Figure 1. Cross-section of an AEM electrolyzer, showing the end plates, GDLs, CLs, and membrane, as well as the location of the water feed and hydrogen and oxygen exits. The line at the bottom denotes the extent of the 1-D model in this work and defines the cathode CL/membrane interface as x=0.

Electrolyte salts, typically potassium hydroxide, can be dissolved into the reactant water to increase its conductivity and improve device performance. Recently, multiple groups have demonstrated AEM electrolysis using potassium carbonate as well as hydroxide electrolytes (5, 6). Carbonate electrolytes are less corrosive than hydroxide electrolytes due to their lower pH; however, the presence of carbonate ions in the AEM results in poorer performance. Performance loss due to incorporation of carbonate ions in the membrane is also seen in AEM fuel cells exposed to carbon dioxide (7, 8).

In this work, a multiphysics model of an AEM electrolyzer is developed to study the effects of carbonate electrolyte on device performance. This work extends the pioneering

modeling work of An *et al.* (9) to include a liquid electrolyte and the effects of carbonate-hydroxide ion exchange. Using the model, we investigate the performance differences observed in AEM electrolyzers using carbonate electrolytes as compared to hydroxide electrolytes. We explore the impact of increased membrane resistance and the effects of a hydroxide concentration gradient caused by carbonate ions in the membrane. We also illustrate the effect of catalyst loading on both the carbonate- and hydroxide-fed electrolyzers.

Theoretical

The 1-D electrolysis cell model used in this work comprises CLs and GDLs on either side of an AEM, with a microporous layer (MPL) between the cathode CL and GDL to match the experimental configuration of Pavel *et al.* (5). Most of the modeling framework and governing equations are adapted from our previously-published AEM fuel cell model (10, 11). Below, we briefly summarize the model, and highlight important changes made to simulate electrolysis.

The model is multiphase, allowing for transport of liquid water, electrolyte ions, and gaseous products through the porous layers. The ionomer in each CL and in the membrane transports water and anions, whereas the liquid electrolyte in the CL and GDL transports cations and anions. The electrochemical model assumes concentration-dependent Butler-Volmer kinetics at each electrode and a hydration-dependent ionic conductivity of the membrane and ionomer. The model was solved at steady state using COMSOL Multiphysics version 5.3a.

Model Description

The primary difference between our earlier fuel-cell model and this work is the existence of a current-carrying liquid electrolyte. Thus, we have added a Nernst-Planck equation to model ion motion in the liquid electrolyte and use a Donnan potential expression to describe ion exchange between the liquid electrolyte and the ionomer. Additionally, due to the presence of aqueous liquid electrolyte, we assume fully humidified gases. Below, we briefly review the relevant equations for transport of gases and liquids within the porous media, as well as ion transport within each electrolyte.

Gas and Liquid Flow. The velocity v_k of the gas or liquid mixture through the porous media is assumed to follow Darcy's Law,

$$v_k = -\frac{K_k}{\mu_k}\nabla p_k, \qquad [4]$$

where μ is the viscosity, K is the permeability, and P is the pressure of phase k (gas or liquid). The viscosity of each mixture and the permeabilities of the GDL, MPL, and CL are calculated as described in our previous work (11, 12).

Gas Transport. The mass flux m_i of each gaseous species i in the porous media is defined as

$$m_i = \rho_g \omega_i v_g - \rho_G \omega_i \sum_j^n \overline{D}_{ij}\left(\nabla x_j + \frac{(x_j-\omega_j)\nabla p_G}{p_G}\right), \qquad [5]$$

where ω_i is the weight fraction and x_i the mole fraction of species i, and $\overline{D}_{ij}$ is an effective binary diffusion coefficient calculated as described in our previous work (11). The first term represents convection and the second represents multicomponent Stefan-Maxwell diffusion.

Transport within the Membrane and Ionomer. The flux of each charged species through the ionomer is influenced by migration, streaming current, and diffusion according to a modified Nernst-Planck equation (10),

$$N_{i,M} = -\frac{\kappa_i y_i}{z_i F}\nabla\phi_2 - \frac{\xi_i \kappa_i y_i}{z_i^2 F^2}\nabla\mu_{H_2O} - D_{i,M} c_t \nabla y_i, \quad [6]$$

where κ_i, z_i, ξ_i, $D_{i,M}$, and y_i are respectively the conductivity, charge, electroosmotic coefficient, diffusion coefficient, and mole fraction of species i within the membrane and ionomer, μ_{H_2O} is the chemical potential of water, and c_t represents the concentration of the fixed positive charge due to the presence of the ionomer. The conductivity of the carbonate and bicarbonate forms of the membrane were assumed equal to each other and to one-fifth of the hydroxide form conductivity:

$$\kappa_{CO_3^{2-}} = \kappa_{HCO_3^-} = 0.2\kappa_{OH^-}, \quad [7]$$

which is consistent with conductivity measurements of various membranes in both forms and the aqueous diffusivities of the ions (7, 13). The total ionic current is given by the sum of the fluxes of each ion,

$$i_2 = \sum_i z_i F N_{i,M}, \quad [8]$$

and the electronic current is given by Ohm's law:

$$i_1 = -\sigma\nabla\phi_1. \quad [9]$$

Transport of water through the membrane is governed by electroosmosis and diffusion down its chemical-potential gradient,

$$N_{\mathrm{H_2O},M} = -\left(\sum_i \frac{\kappa_i \xi_i y_i}{z_i F}\right)\nabla\phi_2 - \left(\alpha_{eff} + \sum_i \frac{\kappa_i \xi_i^2 y_i}{z_i^2 F^2}\right)\nabla\mu_{\mathrm{H_2O},M}. \quad [10]$$

Electrochemical Kinetics. The rates of the hydrogen evolution reaction (HER) and the oxygen evolution reaction (OER) are each modeled by assuming Butler-Volmer kinetics:

$$i_{rxn,HER} = a i_{0,HER}\left[\left(\frac{c_t y_{OH^-}}{c_{ref}}\right)\left(\frac{p_{H_2}}{p_{ref}}\right)^{0.5}\exp\left(\frac{\alpha_{HER,a}F}{RT}\,\eta\right) - a_{H_2O}\exp\left(-\frac{\alpha_{HER,c}F}{RT}\eta\right)\right], \quad [11]$$

$$i_{rxn,OER} = a i_{0,OER}\left[\left(\frac{c_t y_{OH^-}}{c_{ref}}\right)\exp\left(\frac{\alpha_{OER,a}F}{RT}\,\eta\right) - \left(\frac{p_{O_2}}{p_{ref}}\right)a_{H_2O}\exp\left(-\frac{\alpha_{HER,c}F}{RT}\eta\right)\right]. \quad [12]$$

Notably, y_{OH^-} appears in the anodic terms of both Butler-Volmer equations. Thus, a change in y_{OH^-}, as could be caused by ion exchange with a carbonate-containing electrolyte solution, could appear as a kinetic or thermodynamic (Nernstian) voltage loss.

Transport of Ions in Liquid Electrolyte. The presence of an ionically conductive liquid electrolyte differentiates this model from our previously published fuel-cell model. Transport of ions in the electrolyte is governed by the Nernst-Planck equation,

$$N_{i,E} = -D_{i,E}\nabla c_{i,E} - \frac{z_i D_{i,E} F c_{i,E}}{RT}\nabla \phi_3, \quad [13]$$

where $N_{i,E}$ is the molar flux of ions in the electrolyte, $D_{i,E}$ and $c_{i,E}$ represent the diffusivity and concentration of species i in the electrolyte, and ϕ_3 is the ionic potential in the electrolyte. For simplicity, we neglect the small convective contribution to the flux. The diffusivities $D_{i,E}$ of the ions in the electrolyte are computed from the aqueous diffusivities at infinite dilution (13), $D_{i,aq}$, by:

$$D_{i,E} = D_{i,aq}(\epsilon s_L)^{1.5}, \quad [14]$$

where ϵ is the porosity of the solid phase and s_L the liquid saturation.

Ion Exchange between Electrolyte and Ionomer. To model ion exchange between the liquid electrolyte and the ionomer, a first-order rate equation is used, consistent with a Donnan equilibrium between the membrane and the ionomer:

$$R_{exchange,i} = k_{exchange}\left(y_i c_t \exp\left(\frac{z_i F(\phi_2 - \phi_3)}{RT}\right) - c_{i,E}\right), \quad [15]$$

in which $R_{exchange,i}$ represents the rate of ion exchange into the liquid electrolyte from the ionomer, and $k_{exchange}$ is a rate constant set to an arbitrarily large value (100 s^{-1}).

Carbonate Reactions. In addition to ion exchange, carbonate and bicarbonate ions are subject to acid-base equilibrium reactions,

$$HCO_3^- + OH^- \rightarrow CO_3^{2-} + H_2O, \quad [16]$$
$$HCO_3^- \rightarrow CO_2 + OH^-. \quad [17]$$

These reactions occur within both the ionomer and the liquid electrolyte. The rate of carbonate generation from the acid-base reaction (Equation 16) is denoted $R_{CO_3^{2-},gen}$, and the rate of CO_2 desorption from the ionomer is denoted R_{CO_2}. The rates of these reactions are assumed first order and calculated as described in our previous work (11).

Conservation Equations. Considering the electrochemical half-reactions (Equations 2 and 3), the ion-exchange reaction (Equation 15), and the acid-base reactions (Equations 16 and 17), the following conservation equations can be derived for each ion species in the ionomer:

$$\nabla \cdot N_{OH^-,M} = -\frac{i_{rxn}}{F} - R_{exchange,OH^-} + R_{CO_2} - R_{CO_3^{2-},gen}. \quad [18]$$

$$\nabla \cdot N_{HCO_3^-,M} = -R_{exchange,HCO_3^-} - R_{CO_2} - R_{CO_3^{2-},gen}. \quad [19]$$

$$\nabla \cdot N_{CO_3^{2-},M} = -R_{exchange,CO_3^{2-}} + R_{CO_3^{2-},gen}. \quad [20]$$

Within the ionomer in the CLs, water is also produced or consumed by each electrochemical half-reaction, leading to the following conservation equations:

$$\nabla \cdot N_{H_2O,M} = \frac{i_{rxn,OER}}{2F} - R_{MV} - R_{ML}, \text{ anode} \quad [21]$$

$$\nabla \cdot N_{H_2O,M} = \frac{i_{rxn,HER}}{F} - R_{MV} - R_{ML}, \text{ cathode} \quad [22]$$

where R_{MV} and R_{ML} are the rate of water desorption from the ionomer to the vapor or liquid phase as described in our previous work (11).

Boundary Conditions. At the GDL/channel boundaries, gas and liquid pressure are set to 1 atm, gas compositions are set to fully humidified hydrogen at the cathode and fully humidified air (21% O_2, 79% N_2 dry) at the anode, and the temperature is set to 316 K. No-flux boundary conditions are imposed on ionomer-bound species at the CL/GDL boundaries.

Results and Discussion

Validation of Model with Experimental Data

We simulated an AEM electrolyzer under two inlet feed conditions: one with 1 M KOH electrolyte fed to the anode and the other with 1 wt. % K_2CO_3 electrolyte (0.7277 M) fed to the anode. The model reproduces the effect shown in experimental data reported by Pavel *et al*. (5) upon switching from KOH to K_2CO_3 electrolyte, as seen in Figure 2. This fit was achieved using the catalyst parameters given in Table I. The specific surface area of each catalyst layer was set to 10^5 cm^2/cm^3. The CL thickness was calculated from the catalyst loading L, estimated density ρ_{solid}, and pore volume V_{pore} as follows:

$$T_{CL} = L\left(\rho_{solid} + \frac{1}{V_{pore}}\right). \quad [23]$$

TABLE I. Properties of the catalyst layers used in the model.

	Catalyst	Catalyst Loading (mg/cm^2)$^+$	Pore Volume (cm^3/g)$^+$	Density (g/cm^3)*	CL thickness (μm)	Exchange current density (mA/cm^2)
Anode	ACTA 3030	36	0.35	4.0	216	1.0×10^{-4}
Cathode	ACTA 4030	7.4	0.59	5.6	56.9	7.0×10^{-3} †

*Estimated based on information from Pavel *et al.* (5)

$^+$Given by Pavel *et al.* (5)

†Estimated based on measured exchange current densities for non-platinum-group-metal catalysts in alkaline environments (14).

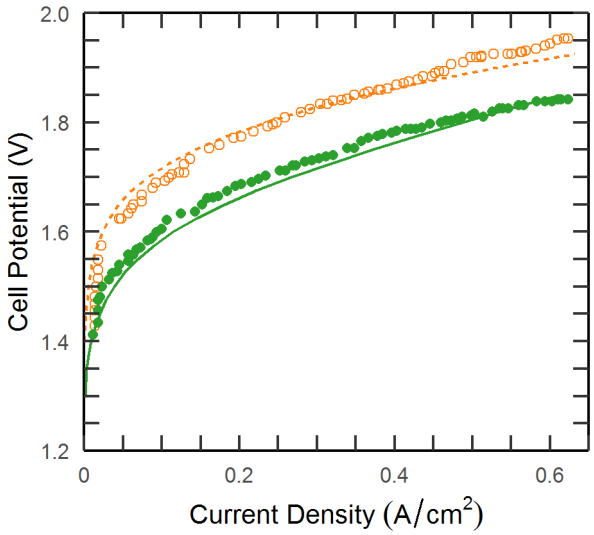

Figure 2. Comparison of model to experimental data. Points (green closed circles for the KOH-fed and orange open circles for the K_2CO_3-fed electrolyzer) represent the experimental data collected by Pavel (5), and lines (solid green for the KOH-fed and dashed orange for the K_2CO_3-fed electrolyzer) represent the values predicted by the model.

Effect of Carbonate Ions on Membrane Conductivity

One possible explanation for the worse performance with carbonate electrolytes is the reduced conductivity of the membrane in carbonate form relative to hydroxide form. Figure 3 shows the effect of reducing or increasing the carbonate-form membrane conductivity by a factor of 5. As shown in the figure, the performance of the electrolyzer is not sensitive to the conductivity of the carbonate-form membrane, indicating that the reduction in conductivity upon exchanging from carbonate to hydroxide form is likely not the primary cause of the increased voltage.

The conductivity of the carbonate-form membrane does not influence performance because carbonate is not the primary charge-carrying ion in the system. Calculation of the hydroxide transference number (Figure 3b) shows that hydroxide current makes up over 95% of the total ionic current in the electrolyte at all current densities. Carbonate ions, however, can influence the cell voltage in other ways by replacing hydroxide in the catalyst layers. We discuss these potential effects below.

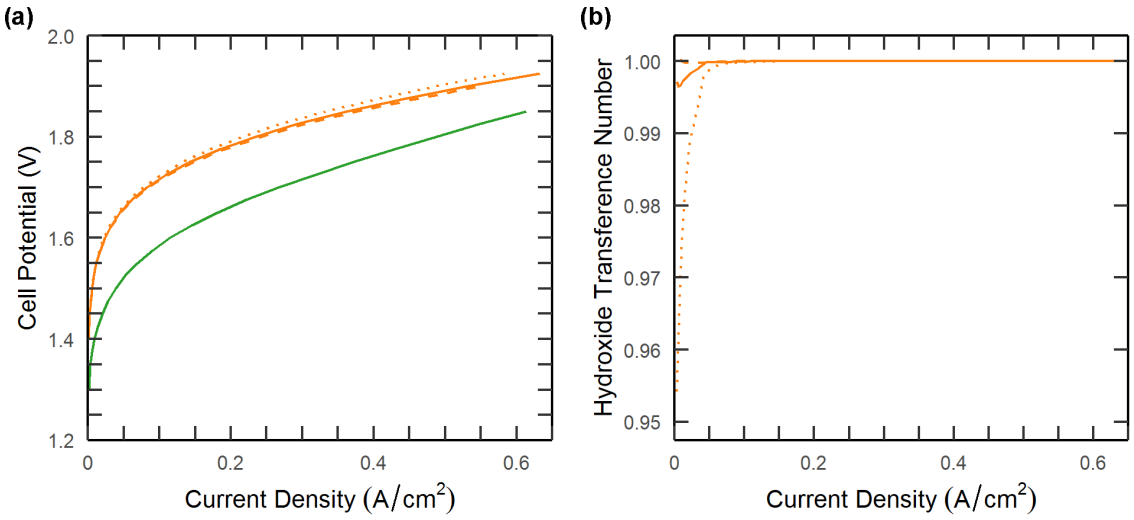

Figure 3. (a) Sensitivity of electrolyzer model to the conductivity of the carbonate-form membrane. Modeled polarization curves of KOH-fed (green) and K_2CO_3-fed electrolyzers (orange) show that when membrane conductivity was either increased (orange dotted line) or decreased (orange dashed line) by a factor of 5 relative to the baseline model (orange solid line), performance for a K_2CO_3 electrolyzer hardly varied. The membrane conductivity change thus fails to explain the observed voltage increase relative to the KOH-fed electrolyzer (green line). (b) Hydroxide transference number for the K_2CO_3-fed electrolyzer for each carbonate-form conductivity.

Polarization Due to Hydroxide Redistribution

A hydroxide concentration gradient, caused by the presence of carbonate ions, can result in a Nernstian voltage loss across AEM fuel cells exposed to carbon dioxide (7, 11, 15, 16). Such a hydroxide concentration gradient is likely also present in AEM electrolyzers with carbonate electrolytes. Figure 4 reports the mole fraction of hydroxide ions in carbonate-fed electrolyzers. With hydroxide electrolyte, the hydroxide mole fraction in the ionomer remains constant, so no Nernstian overpotential is observed. In contrast, the carbonate ions in the K_2CO_3 electrolyzer cause the hydroxide mole fraction to vary throughout the cell.

The Nernst equation can associate this non-uniform distribution of hydroxide with an overpotential roughly equivalent to the performance difference between carbonate- and hydroxide-fed electrolyzers. The Nernst equation defines the overpotential created by a hydroxide concentration difference from cathode to anode as:

$$\Delta V_{Nernst} = \frac{RT}{F} \ln \frac{y_{OH^-,c}}{y_{OH^-,a}}. \quad [24]$$

Using this equation, a concentration drop by a factor of 25 across the ionomer, as calculated by the ratio of the maximum and minimum hydroxide concentrations seen in the ionomer at 1.7 V, produces a voltage loss of 0.088 V, which is approximately the voltage difference between carbonate and hydroxide-fed electrolyzers at 100 mA/cm^2 current density. This concentration difference is comparable in magnitude to that observed for carbonate-fed electrolyzers in Figure 4, indicating that the additional voltage required with carbonate

electrolytes is likely due to Nernstian overpotential effects rather than a reduction in membrane conductivity.

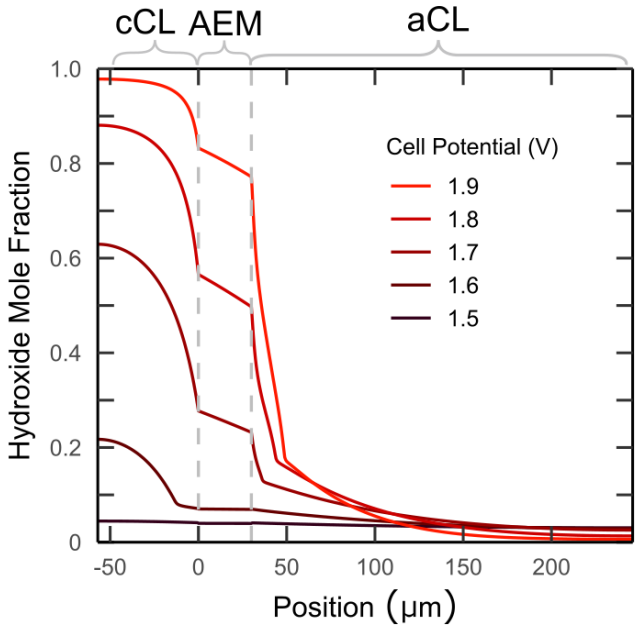

Figure 4. Hydroxide mole fraction within the ionomer and membrane of an AEM electrolyzer with K_2CO_3 electrolyte. Dashed gray lines mark the position of the AEM; the cathode CL is to the left of the AEM and the anode CL to the right.

Furthermore, as shown in Figure 4, the membrane contains a significant fraction of hydroxide ions, particularly at high voltage, due to the production of hydroxide anions in the cathode. Thus, the membrane remains at least partially in hydroxide form during operation, which helps explain the insensitivity to conductivity of the carbonate-form membrane demonstrated earlier. This so-called "self-purging" phenomenon is also commonly observed in AEM fuel cells, in which hydroxide produced at the cathode displaces carbonate and improves membrane conductivity (7, 16, 17).

Blocking of Catalyst Layer due to Carbonates in the Anode

By reducing the availability of hydroxide, carbonate ions also alter the utilization of the anode catalyst. Figure 5 shows the reaction rates along the anode CL for the KOH and K_2CO_3 electrolyzers, normalized to average current density through the cell,

$$i_{rxn,norm} = \frac{\tau_{CL} i_{rxn}}{i_{cell}}. \qquad [25]$$

At high cell potential, most of the reaction in the K_2CO_3 electrolyzer occurs right next to the membrane, while in the KOH electrolyzer, reaction is more spread out along the length of the CL. The decreased catalyst utilization in the K_2CO_3 electrolyzer is a direct result of the reduced hydroxide concentration in the anode, because the OER requires hydroxide.

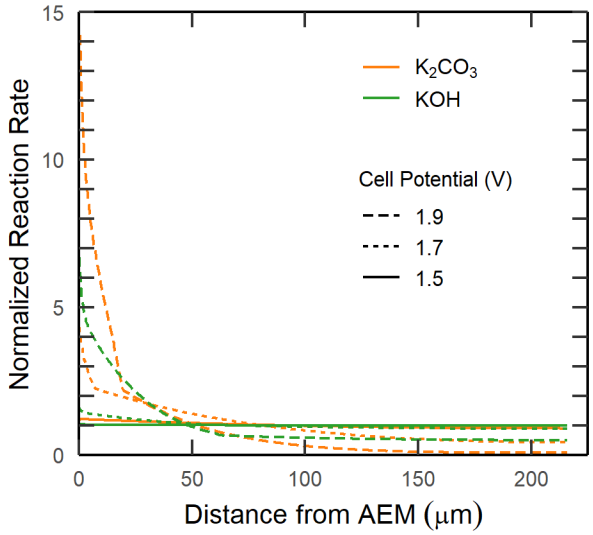

Figure 5. Normalized reaction rate within the anode CL of the AEM electrolyzer with KOH electrolyte (green) and K_2CO_3 electrolyte (orange). The reaction tends to be localized nearer to the membrane when using K_2CO_3 electrolytes due to carbonate accumulation in the anode, which reduces catalyst utilization.

Catalyst-Layer Thickness

The CL thickness has an effect on the polarization performance of both the KOH and K_2CO_3 electrolyzer. Successful calibration of our model required the use of 216 μm of catalyst on the anode and 56.9 μm of catalyst on the cathode. These catalyst layer thicknesses were estimated from the properties of the catalysts used (see Table 1 and Equation 23). Scanning electron micrographs of electrolyzer CLs at similar catalyst loadings suggest CL thicknesses of 670 μm on the anode and 118 μm on the cathode, although with a different binder (18). Figure 6 shows the result of reducing CL thickness to 20 μm, which represents a significant decrease in catalyst loading and potentially a decrease in device cost.

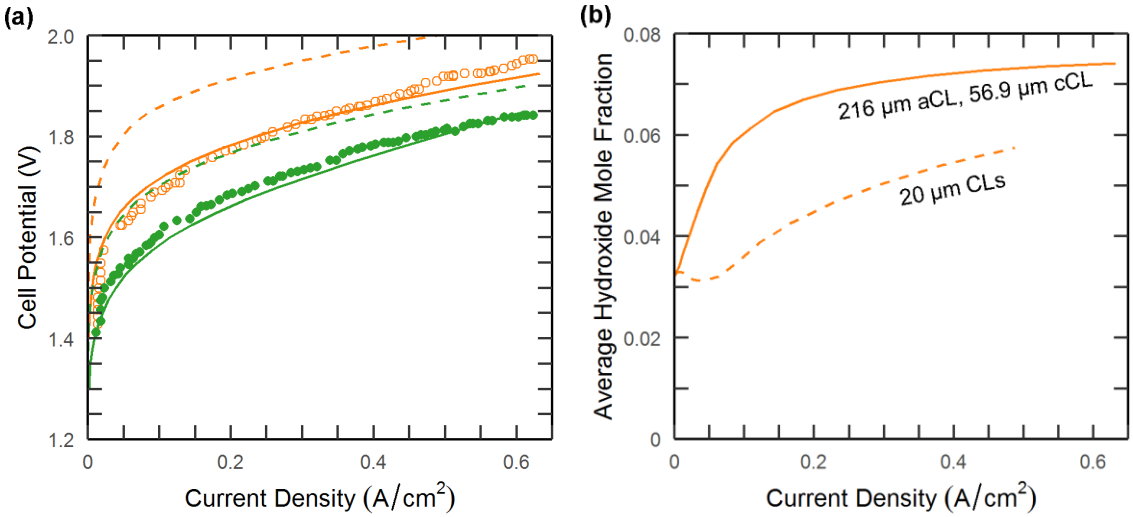

Figure 6. (a) The effect of reduced anode and cathode catalyst loading. Solid lines indicate our earlier model fits for KOH-fed (green) and K_2CO_3-fed electrolyzers using CL

thicknesses of 216 and 56.9 μm on the anode and cathode, respectively. Dashed lines indicate the polarization response for 20 μm thick CLs on both anode and cathode. (b) Average hydroxide mole fraction in the anode CL for K_2CO_3-fed electrolyzers with each set of CL thickness values.

As seen in the figure, reducing CL thickness increases cell potential at all current densities due to increased kinetic polarization losses. The effect is slightly more pronounced for the K_2CO_3-fed electrolyzer, particularly at higher current densities. Our model also shows that the replacement of carbonate ions in the anode CL with hydroxide (the self-purging effect) is less effective for thinner CLs (figure 6b). These results suggest that the enhancement of the kinetic losses in the K_2CO_3-fed electrolyzer is due to reduced hydroxide content in the thinner CL.

Conclusions

In this work, we developed a mathematical model to compare the performance of an anion-exchange-membrane electrolyzer fed with potassium hydroxide electrolyte to one fed with potassium carbonate electrolyte. Our results suggest that the loss in conductivity when carbonates replace hydroxide in the membrane has little effect on the performance of the device, likely due to the displacement of carbonate ions in the membrane by hydroxide produced in the cathode. Instead, the decrease in hydroxide content in the anode ionomer is a primary cause of the performance difference between KOH and K_2CO_3 electrolyzers. This reduction in hydroxide content results in a Nernstian voltage penalty. Furthermore, carbonates pile up near the GDL/CL interface during operation, reducing catalyst utilization by forcing the oxygen evolution reaction to occur nearer the membrane interface. These effects are exacerbated by reduced catalyst loading and highlight the importance of catalyst layer and electrolyte design in AEM electrolysis systems.

Acknowledgements

This work was supported in part by the U.S. Department of Energy, Office of Science, Office of Workforce Development for Teachers and Scientists (WDTS) under the Science Undergraduate Laboratory Internship (SULI) program, as well as by the Assistant Secretary for Energy Efficiency and Renewable Energy, Fuel Cell Technologies Office, of the U.S. Department of Energy under contract number DE-AC02-05CH11231. We also thank Sanjeev Mukerjee, Ian Kendrick, Andrew Crothers, Lien-Chun Weng, and Nemanja Danilovic for helpful discussions.

Nomenclature

$\bar{D}_{ij}$	Stefan-Maxwell binary diffusion coefficient between species i and j (cm^2/s)
$D_{i,E}$	Diffusion coefficient of species i within the electrolyte (cm^2/s)
$D_{i,M}$	Diffusion coefficient of species i within the membrane or ionomer (cm^2/s)
F	Faraday's constant (C/mol)
i	Current density (A/cm^2)
m_i	Mass flux of species i ($kg\ m^{-2}\ s^{-1}$)
K_k	Permeability of phase k (m^2)
N	Molar flux ($mol\ cm^{-2}\ s^{-1}$)

p_k Pressure of phase k (Pa)
R Gas law constant (J/mol)
T Temperature (K)
T_{CL} Catalyst layer thickness (μm)
v_k Velocity of phase k (m/s)
x_i Mole fraction of species i in the gas phase
y_i Mole fraction of species i in the membrane or ionomer

Greek Letters
α Water transport coefficient ($mol^2\ J^{-1}\ cm^{-1}\ s^{-1}$)
ϵ Porosity
η Overpotential (V)
κ Ionic conductivity (S/cm)
μ_{H_2O} Water chemical potential (J/mol)
ξ Electro-osmotic coefficient
ρ Density (g/cm^3)
Φ Electric potential (V)
ω Mass fraction

Subscripts
a anode
c cathode
G gas
L liquid
HER hydrogen evolution reaction
OER oxygen evolution reaction

References

1. U. S. Department of Energy, Hydrogen Production: Natural Gas Reforming, https://www.energy.gov/eere/fuelcells/hydrogen-production-natural-gas-reforming (accessed December 2018).
2. I. Vincent and D. Bessarabov, *Renewable and Sustainable Energy Reviews*, **81**, 1690 (2018).
3. M. Carmo, D. L. Fritz, J. Mergel and D. Stolten, *International Journal of Hydrogen Energy*, **38**, 4901 (2013).
4. R. Abbasi, B. P. Setzler, S. Lin, J. Wang, Y. Zhao, H. Xu, B. Pivovar, B. Tian, X. Chen, G. Wu and Y. Yan, *Adv Mater*, 1805876 (2019).
5. C. C. Pavel, F. Cecconi, C. Emiliani, S. Santiccioli, A. Scaffidi, S. Catanorchi and M. Comotti, *Angewandte Chemie - International Edition*, **53**, 1378 (2014).
6. H. Ito, N. Kawaguchi, S. Someya, T. Munakata, N. Miyazaki, M. Ishida and A. Nakano, *International Journal of Hydrogen Energy*, **43**, 17030 (2018).
7. N. Ziv, W. E. Mustain and D. R. Dekel, *ChemSusChem*, **11**, 1136 (2018).
8. G. Li, Y. Wang, J. Pan, J. Han, Q. Liu, X. Li, P. Li, C. Chen, L. Xiao, J. Lu and L. Zhuang, *International Journal of Hydrogen Energy*, **40**, 6655 (2015).
9. L. An, T. S. Zhao, Z. H. Chai, P. Tan and L. Zeng, *International Journal of Hydrogen Energy*, **39**, 19869 (2014).
10. H.-S. Shiau, I. V. Zenyuk and A. Z. Weber, *Journal of The Electrochemical Society*, **164**, E3583 (2017).

11. M. R. Gerhardt, L. M. Pant and A. Z. Weber, *Journal of The Electrochemical Society*, **166**, F3180 (2019).
12. I. V. Zenyuk, P. K. Das and A. Z. Weber, *Journal of The Electrochemical Society*, **163**, F691 (2016).
13. P. Vanysek, Ionic Conductivity and Diffusion at Infinite Dilution, in *CRC Handbook of Chemistry and Physics*, 99th Edition ed., J. R. Rumble Editor, CRC Press/Taylor & Francis, Boca Raton, FL (2019).
14. S. M. Alia and B. S. Pivovar, *Journal of The Electrochemical Society*, **165**, F441 (2018).
15. U. Krewer, C. Weinzierl, N. Ziv and D. R. Dekel, *Electrochimica Acta*, **263**, 433 (2018).
16. M. Inaba, Y. Matsui, M. Saito, A. Tasaka, K. Fukuta, S. Watanabe and H. Yanagi, *Electrochemistry*, **79**, 322 (2011).
17. N. Ziv and D. R. Dekel, *Electrochemistry Communications*, **88**, 109 (2018).
18. I. Vincent, A. Kruger and D. Bessarabov, *International Journal of Hydrogen Energy*, **42**, 10752 (2017).